Opto-Electronic Science

Original Article

2022, Vol. 1, No. 6

DOI: 10.29026/oes.2022.210013

Giant and light modifiable third-order optical nonlinearity in a free-standing h-BN film

Jun Ren[1,2], Han Lin[1,5,6], Xiaorui Zheng[1], Weiwei Lei[3], Dan Liu[3], Tianling Ren[2], Pu Wang[4] and Baohua Jia[1,5,6]*

Recently, hexagonal boron nitride (h-BN) has become a promising nanophotonic platform for on-chip information devices due to the practicability in generating optically stable, ultra-bright quantum emitters. For an integrated information-processing chip, high optical nonlinearity is indispensable for various fundamental functionalities, such as all-optical modulation, high order harmonic generation, optical switching and so on. Here we study the third-order optical nonlinearity of free-standing h-BN thin films, which is an ideal platform for on-chip integration and device formation without the need of transfer. The films were synthesized by a solution-based method with abundant functional groups enabling high third-order optical nonlinearity. Unlike the highly inert pristine h-BN films synthesized by conventional methods, the free-standing h-BN films could be locally oxidized upon tailored femtosecond laser irradiation, which further enhances the third-order nonlinearity, especially the nonlinear refraction index, by more than 20 times. The combination of the free-standing h-BN films with laser activation and patterning capability establishes a new promising platform for high performance on-chip photonic devices with modifiable optical performance.

Keywords: hexagonal boron nitride; third-order nonlinearity; laser oxidation; optoelectronic device

Ren J, Lin H, Zheng XR, Lei WW, Liu D et al. Giant and light modifiable third-order optical nonlinearity in a free-standing h-BN film. *Opto-Electron Sci* **1**, 210013 (2022).

Introduction

Since the discovery of graphene, more and more two-dimensional (2D) materials have realized diverse applications in electrical and optical devices[1–15]. Hexagonal boron nitride (h-BN) nanosheets, due to their excellent mechanical strength, good thermal conductivity, and high thermal stability, have attracted significant attentions for solid-state thermal neutron detectors, protective coatings and dielectric layers. Furthermore, because of its wide bandgap in the UV region, h-BN has broad potential applications in deep UV light emitters and lasers[16–18], transparent membranes, making it advanced among 2D materials. In particular, h-BN with hyperbolic phonon-polaritons, enabling infrared photonics and optically stable, ultra-bright quantum emitters have been demonstrated recently[19,20], which makes h-BN a promising and versatile nanophotonic platform for all-optical integrated information-processing and communication

[1]Centre for Translational Atomaterials, School of Science, Computing and Engineering Technologies, Swinburne University of Technology, P. O. Box 218, Hawthorn, Victoria 3122, Australia; [2]School of Integrated circuits, Tsinghua University, Haidian, Beijing 100084, China; [3]Institute for Frontier Materials, Deakin University, Geelong, Victoria 3216, Australia; [4]Institute of Laser Engineering, Beijing University of Technology, Chaoyang, Beijing 100124, China; [5]The Australian Research Council (ARC) Industrial Transformation Training, Centre in Surface Engineering for Advanced Materials (SEAM), Swinburne University of Technology, Hawthorn, Victoria 3122, Australia; [6]School of Science, RMIT University, Melbourne, Victoria 3000, Australia.

*Correspondence: BH Jia, E-mail: bjia@swin.edu.au

Received: 17 November 2021; Accepted: 5 January 2022; Published online: 21 June 2022

Open Access This article is licensed under a Creative Commons Attribution 4.0 International License.
To view a copy of this license, visit http://creativecommons.org/licenses/by/4.0/.

© The Author(s) 2022. Published by Institute of Optics and Electronics, Chinese Academy of Sciences.

chip.

Different methods have been carried out for the exfoliation and synthesis of h-BN, such as chemical vapor deposition (CVD), metal-organic vapor phase epitaxy (MOVPE), pulsed laser deposition (PLD), mechanical exfoliation or liquid exfoliation method[21]. In these systems, h-BN films were measured on different substrates, which render the films not readily integratable with any functional devices without sophisticated transferring process. On the other hand, exciting quantum emitting and nanophotonic devices have been demonstrated on free-standing platforms[19,20] due to the better light confinement in such a comparatively lower refractive index (~1.7) material and the unique high mechanical strength of the h-BN thin film[19]. Thus, free-standing h-BN films are highly preferred in functional device integration.

Optical nonlinearity of h-BN materials has been reported by researchers. Li et al. established a second harmonic generation (SHG) system as a precise optical probe to measure the SHG intensity in few-layer h-BN[22]. The effective volume second-order nonlinear susceptibility of h-BN was as high as $d_{\text{h-BN}}$=9.1×10^{-23} C/V^2, which was comparable to that of transparent nonlinear crystals such as $LiNbO_3$ and β-BaB_2O_4. Kim et al. further reported thick h-BN flakes with 100 layers showing strong SHG similar to few-layer h-BN, confirming that thick h-BN flakes can serve as a nonlinear optical platform with its advantage of easy exfoliation[23]. Popkova et al. first reported third-order nonlinearity of h-BN flakes with thicknesses ranging from 5 to 170 nm, determining that the h-BN third-order susceptibility $\chi^{(3)}$=8.4×10^{-21} m^2/V^2, which is comparable to the cubic susceptibility of Si_3N_4[24]. For all-optical communication systems, high optical nonlinearity is essential. Studies have shown h-BN aqueous solution and few-layer nanosheets both possess giant third-order nonlinearity under different laser irradiation with different pulse widths of nanosecond, picosecond and femtosecond.

In this paper, using a unique solution-based large-scale synthesize method, we developed free-standing h-BN films with high mechanical strength[25]. The third-order optical nonlinearity of such free-standing h-BN thin films was revealed and their complex nonlinear susceptibility $\chi^{(3)}$ was characterized by using the Z-scan technique. We report, for the first time, laser modified optical nonlinearity in a free-standing h-BN film, which significantly enhances the nonlinear refraction index n_2 by more than 20 times. Through analyzing the material responses by infrared and Raman spectroscopy, the modification mechanism was revealed. Efficient frequency conversion has been demonstrated with a four-wave mixing (FWM) system, showing the giant third-order nonlinear susceptibility of h-BN towards state-of-the-art functional nonlinear h-BN devices. Flexible micro-patterns were, for the first time, introduced by femtosecond direct laser writing, adding tremendous devising functionalities to the system. Our results demonstrate the free-standing h-BN film can be a promising and highly versatile platform for on-chip nonlinear photonic devices, and the laser modification and patterning allow further modification of the functions of the devices, which will find broad photonics applications[26,27].

Preparation of h-BN films and flexible laser patterning

The free-standing h-BN thin films were synthesized by a solution-based method[25]. Commercially available h-BN powder was applied for the following one-step ball milling exfoliation method. After ball milling, vacuum-assisted filtration process was used to obtain the h-BN thin film. After filtrated, the h-BN film can be easily peeled off unbrokenly into a freestanding state, indicating its good mechanical strength and making it flexible for further application, as shown in Fig. 1(a). The thickness, which is a key parameter of photonic devices applications, can be accurately controlled by the amount of solution used in the filtration process. In this paper, a 3 μm-thick h-BN thin film has been used for the optical measurements. Transmission electron microscopy (TEM) image of the h-BN nanosheets is shown in Fig. 1(b), suggesting that the h-BN nanosheets are flat and thin. The high-resolution TEM (HRTEM) image has clearly shown five stacked h-BN layers in the sample, as seen in Fig. 1(c).

To introduce strong laser-h-BN film interaction, femtosecond laser pulses (20×10^3 μJ/cm^2) at λ=800 nm with a low repetition rate (1 kHz) were focused using an objective lens with NA=0.8[28,29]. Due to the massive localized energy in the focal region, the h-BN material was significantly modified. As a result, flexibly designed micropatterns can be readily introduced into the film through direct laser writing. A vivid Australian map with a size of 50 μm × 50 μm can be fabricated on the h-BN thin film (Fig. 1(d)). This is the first demonstration of laser fabrication of arbitrary micropatterns in an h-BN

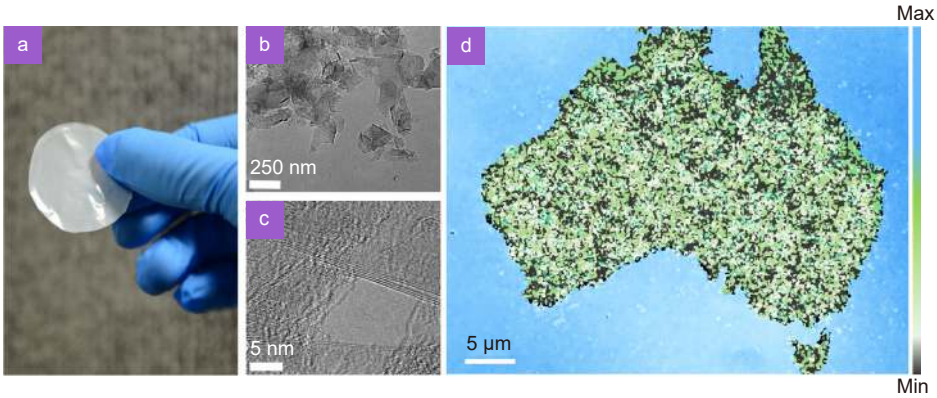

Fig. 1 | (**a**) Photo of the freestanding vacuum-assisted filtrated h-BN film. (**b**) TEM image of the prepared h-BN nanosheets by drop coating the ball-milled h-BN solution on a carbon-coated copper grid. (**c**) HRTEM image of the h-BN nanosheets with five layers. (**d**) Laser patterned micro-pattern of an Australian map on a free-standing h-BN film.

film, showing its great potential for direct device formation for optoelectronic and photonic applications.

Mechanism of laser patterning

The laser patterning capability of hBN provides enormous flexibility for it to directly serve as functional optoelectronic devices by functional nanostructure fabrication. To reveal the fundamental process of laser interaction with h-BN and achieve a better control of the material and structural properties, Fourier transform infrared (FTIR) spectroscopy is applied to measure the characteristic peaks of different functional groups. The FTIR spectra show the evolution of the chemical bonds before and after the laser irradiation (fluence = 20×10^3 μJ/cm^2) in Fig. 2(a), which indicate that laser irradiation leads to effective oxidation in the h-BN film. For pristine h-BN film, a peak at 1362 cm^{-1} stands for in-plane B-N stretching vibration mode and another peak at 818 cm^{-1} stands for B-N-B bending vibration mode. An additional peak at 3303 cm^{-1} is attributed to the N-H and O-H bonds at the edge planes of h-BN or the surface moisture. Once irradiated by the femtosecond laser, another peak

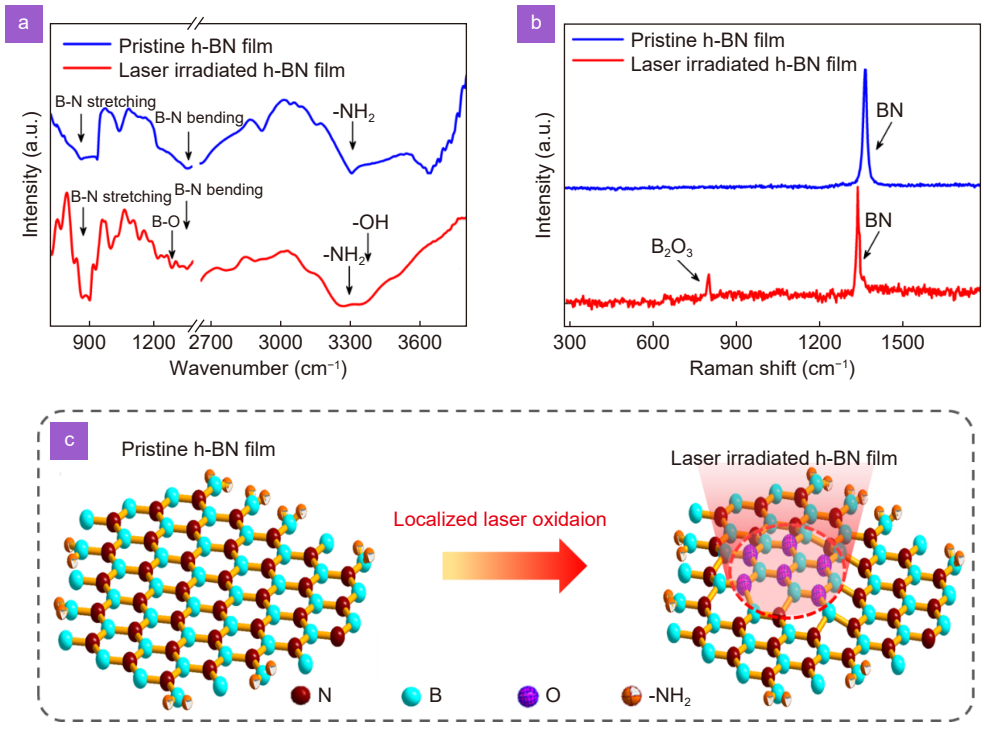

Fig. 2 | (**a**) FTIR spectra of the pristine h-BN film (blue line) and laser irradiated h-BN film (red line). (**b**) Raman spectra with laser excitation at the wavelength of 532 nm of the pristine h-BN film (blue line) and laser irradiated h-BN film (red line). (**c**) Atomic structure of pristine h-BN film and localized oxidation area after laser irradiation (red dash area).

appeared at 1260 cm^{-1} due to the formation of O-B-O bonds[30]. Meanwhile, the peak around 3303 cm^{-1} is strongly increased and broadened as a result of the overlap of O-H bonds and N-H bonds that are enhanced during the oxidation process. Such h-BN oxidation behavior in ambient environments upon high thermal treatment is similar to the previous observations.

The oxygen-containing groups, formed due to the laser irradiation, can also be confirmed from the Raman spectra shown in Fig. 2(b). Before laser irradiation, the h-BN film contains the counter-phase B-N vibrational mode E_{2g}, locating at 1366 cm^{-1}. After laser treatment, the B-N vibrational peak is shifted to a lower wavenumber of 1356 cm^{-1} and a second signal appears at 810 cm^{-1}, which is assigned to be the B-O bond. After laser irradiation, the intensity decreased due to two reasons: 1) the thickness of the film decreased by 10% due to the ablation of h-BN film by the laser beam, 2) the surface roughness became higher, which increased scattering of the signal. As a result, the noise level is relatively higher after laser radiation. It has been reported when exposed to high temperature (800–900 °C), h-BN would be oxidized to boron oxide, as the following Eqs. (1) and (2)[31]:

$$4BN\,(s) + 3O_2 \rightarrow 2B_2O_3\,(I) + 2N_2\,(g)\ , \qquad (1)$$

$$2BN\,(s) + 3H_2O\,(g) \rightarrow B_2O_3\,(I) + 3H_2\,(g) + N_2\,(g)\ . \qquad (2)$$

As illustrated in Fig. 2(c), as a member of the 2D material family, B and N atoms arranging in a sp^2-bonded hexagonal lattice structure in-plane consist of h-BN nanosheets, and layered sheets are stacked by van der Waals interactions. Upon tightly focused laser beam irradiation, local temperature is dramatically increased heating up the lattice. As a result, oxidation process occurs removing the nitrogen atoms and replace with oxygen-containing functional groups attached to the basal flakes and form new chemical groups of B-O bonds. Once oxidized, the sp^3-bonds are significantly enhanced as the increase of the oxygen containing groups. It is expected that the hybridization of the sp^2 and sp^3 atomic clusters will increase the density of electron-hole puddles, rendering different carrier transfers therefore significantly altering the nonlinear response of the h-BN film.

Linear optical properties of laser modified free-standing h-BN films

Like the case in laser-induced reaction in graphene oxide, black phosphorus and other kinds of 2D materials[32–37], such a significant molecular change could cause substantial physical property variation of the h-BN film, including the bandgap, linear and nonlinear optical properties, which can enable additional modification. To this end, the linear optical absorbance and optical constants (refractive index n_0 and extinction coefficient κ) are firstly characterized for both the pristine and the oxidized area of the h-BN film, as shown in Fig. 3(a–c).

The optical absorbance of the freestanding film was measured by ultraviolet-visible (UV-VIS) spectrometer and is shown in Fig. 3(a). For the pristine free-standing h-BN film, the measured absorbance peak presents at a far UV wavelength of 209 nm, showing a large bandgap of 3.8 eV by fitting the Tauc's equation near its cut-off wavelength[38]. Meanwhile, its optical transmittance retains high from 500 nm to infrared wavelength, rendering it an excellent broadband low loss optical material for highly efficient UV shielding/protection and nonlinear applications[39]. After laser irradiation, the absorbance is increased to 0.1, and the absorbance peak is shifted to 300 nm. Meanwhile, the bandgap is changed to 3.1 eV, indicating the different carrier transition mechanism[40]. Remarkably, the bandgap could be flexibly changed in

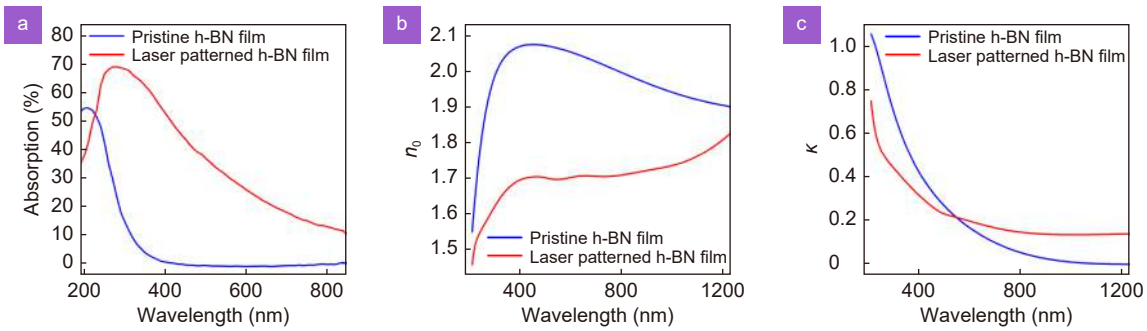

Fig. 3 | (**a**) UV-VIS absorption characterization in the pristine h-BN film (blue line) and the laser patterned area (red line). (**b**) The refractive index (n_0) of the pristine h-BN film (blue line) and laser patterned area (red line). (**c**) The extinction coefficient (κ) of the pristine h-BN film (blue line) and laser patterned area (red line).

the straightforward procedure enabled by laser irradiation, which would open up new applications in many areas such as gas sensors and novel electronic devices[40,41].

Spectroscopic ellipsometer (SE) was used to quantify n_0 and κ for the film from UV to near-infrared range both before and after the laser oxidation, as shown in Fig. 3(b) and 3(c). The refractive index of pristine film is 2.0 at the visible wavelength range, which is the typical value of h-BN materials. After laser oxidation, it decreases obviously, and the refractive index difference is as large as 0.3 in 800 nm. Meanwhile, κ for the pristine h-BN film above 800 nm is negligible, which means that there is almost no material absorption in the near-infrared wavelength range. After oxidation, κ increases to 0.2 in the visible range, showing a similar trend compared to the UV-Vis measurements. Such substantial variations in n_0 and κ offer the essential modulation mechanism for highly efficient phase and amplitude modification for designing ultrathin h-BN optical elements.

Optical properties strongly depend on the material composition. As described in Eqs. (1) and (2), upon laser radiation, the BN material is converted to B_2O_3. The refractive index of pristine B_2O_3 is 1.458[42], which is much lower than pristine h-BN (~2.0). Since the laser did not fully convert h-BN to B_2O_3, the resulted refractive index after laser irradiated was between the value of h-BN and B_2O_3, as shown in Fig. 3(b). In addition, the surface roughness was increased upon laser oxidation as shown in Fig. 1(d), which promoted the absorption in Fig. 3(a). As a result, the absorption increased after laser patterning.

Nonlinear optical properties of laser modified free-standing h-BN films

To explicitly measure the third-order nonlinear coefficient of the h-BN film, a microscopic Z-scan setup similar to that used in our previous experiment[32,43–45] was employed to evaluate the real part (close aperture Z-scan) and imaginary part (open aperture Z-scan) of $\chi^{(3)}$. The experimental results are presented in Fig. 4. When increasing the fluence from 4.6×10^3 μJ/cm² to 15.4×10^3 μJ/cm², the nonlinear absorption behavior maintained and the modulation depth increased from 2% to 16%, as shown in Fig. 4(a), indicating the superior nonlinearities compared with various 2D materials[30,46]. Meanwhile, a pronounced valley-peak pattern is observed in the close

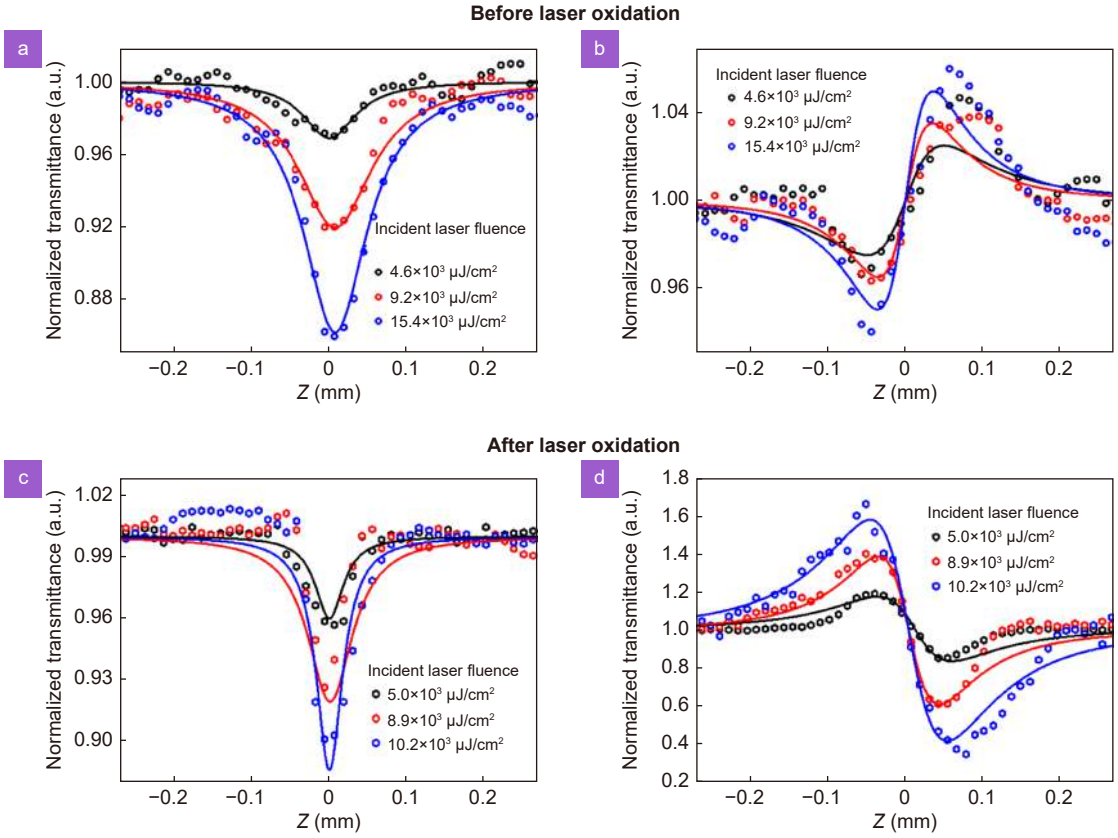

Fig. 4 | (**a**) Open aperture Z-scan results before laser oxidation. (**b**) Close aperture Z-scan results before laser oxidation. (**c**) Open aperture Z-scan results after laser irradiated optical breakdown. (**d**) Close aperture Z-scan result after laser oxidation.

aperture Z-scan results, indicating a positive nonlinear refractive index n_2 (self-focusing) for the pristine free-standing h-BN film, as shown in Fig. 4(b).

When increasing the laser fluence to 18.9×10³ μJ/cm², it is hard to maintain the reversible nonlinear behaviors (result not shown) of the film, indicating a material modification induced by laser radiation started to occur. When further increasing the laser fluence higher than 24×10³ μJ/cm², the ultrahigh pulse energy led to optical breakdown of the h-BN film. From the above-mentioned different processes, we further characterized the optical nonlinearity in the irreversible domain by exploiting the Z-scan laser as a localized laser irradiation source with a fluence of 20×10³ μJ/cm². The open and close aperture Z-scan measurement results are shown in Fig. 4(c) and 4(d). Surprisingly, the nonlinear responses of the laser-oxidized area have been significantly enhanced and most interestingly, the sign of the nonlinear refractive index has been completely reversed. From the open-aperture measurement, both the nonlinear absorption for pristine h-BN and laser oxidized h-BN show a similar optical limiting strength. However, for the close-aperture measurement, the results were totally reversed, which was flipped from valley-peak to peak-valley configuration, indicating the nonlinear refractive index from self-focusing to self-defocusing. Most importantly, the calculated nonlinear refraction has been enhanced orders of magnitude after laser oxidation.

Unlike the intrinsic h-BN, which has sp^2 hybridized π conjugated B and N atoms, the oxidized h-BN has both sp^2 and sp^3 atomic domains by means of attached functional groups on the basal plane or at the edge. Thus, the chemical, electrical and linear optical properties have been changed drastically. Previous studies on graphene/graphene oxide (GO) materials[32–34] suggest that the optical nonlinearity is a strong dependent on the presence of functional groups, no matter covalently or non-covalently bonded. The energy bandgap of sp^2 matrix is low and is saturated due to bleaching of the valance band, while energy bandgap of sp^3 matrix is high and electrons in the valance band pumped to conduction band by two-photon absorption (TPA) and become free carriers. Meanwhile, the electron in the ground state is pumped to the excited state by excited state absorption (ESA). The nonlinear optical enhancement in the oxidized h-BN can be attributed to a combination of TPA, ESA, charge transfer and the enhanced thermal lensing effect after laser oxidation.

To further elucidate the differences between the nonlinear responses for the pristine free-standing h-BN film and the laser modified film, the open and close aperture Z-scan curves are fitted, as presented in Fig. 4(a–d) (solid line), and β (nonlinear absorption coefficient) and n_2 are quantified as the following equation:

β is quantified with the fitting formula[44]:

$$T = \sum_{m=0}^{\infty} \frac{[-q_0(z,0)]^m}{(m+1)^{1.5}} (m \in N) ,$$
$$q_0(z,0) = \frac{\beta \cdot L_{\text{eff}} I_0}{(1+z^2/z_0^2)} . \quad (3)$$

And n_2 is quantified with the fitting formula[47]:

$$T = 1 + \frac{4 \cdot k \cdot L_{\text{eff}} \cdot \gamma \cdot I_0 \cdot x}{z_0} \cdot \left[\left(\frac{x^2}{z_0^2}+9\right)\cdot\left(\frac{x^2}{z_0^2}+1\right)\right]^{-1} ,$$
$$n_2 = c n_0 \gamma / 40\pi . \quad (4)$$

In which $L_{\text{eff}}=(1\text{-}e^{-\alpha L})/\alpha$ is the effective length, L is the sample length, I_0 is the power fluence at the focal point, α is the linear absorption coefficient, c is the velocity of light in vacuum and n_0 is the linear refractive index. γ is the third-order nonlinear refractive index in MSK unit system (meter, kilogram, and second), n_2 is the third-order nonlinear refractive index in esu system.

From Fig. 5(a) and 5(b), as the increase of incident laser fluence, both the calculated n_2 and β vary for the pristine film. When the incident fluence is low, the bound-electronic nonlinearity, the free-carrier nonlinearity and excited-carrier nonlinearity are the main factors of the third-order nonlinearity. However, with the increase fluence of the incident light, the depletion of electrons at the conduction band weakens the contribution from the bound-electronic nonlinearity, leading to the saturation of optical nonlinearity at higher laser fluence, thus making the nonlinear refractive index an intensity dependent parameter.

The "bound-electronic" effect is governed by

$$n(I) = n_0(I) + \Delta n(I) = n_0(I) + n_{2\text{b-e}} I , \quad (5)$$

where I is the input intensity, n_0 is the linear refraction index and $n_{2\text{b-e}}$ is the nonlinear refraction response due to the bound-electronic nonlinearity.[48]

The "free-carrier nonlinearity" follows

$$\Delta n(t) = n_{2\text{free}} I(t) + \sigma_\gamma N(t) , \quad (6)$$

where σ_γ is the free carrier nonlinear coefficient and $N(t)$ is the temporal free carrier density. And t is the time.

The "excited-carrier nonlinearities" (mainly two-photon absorption (2PA)) follows

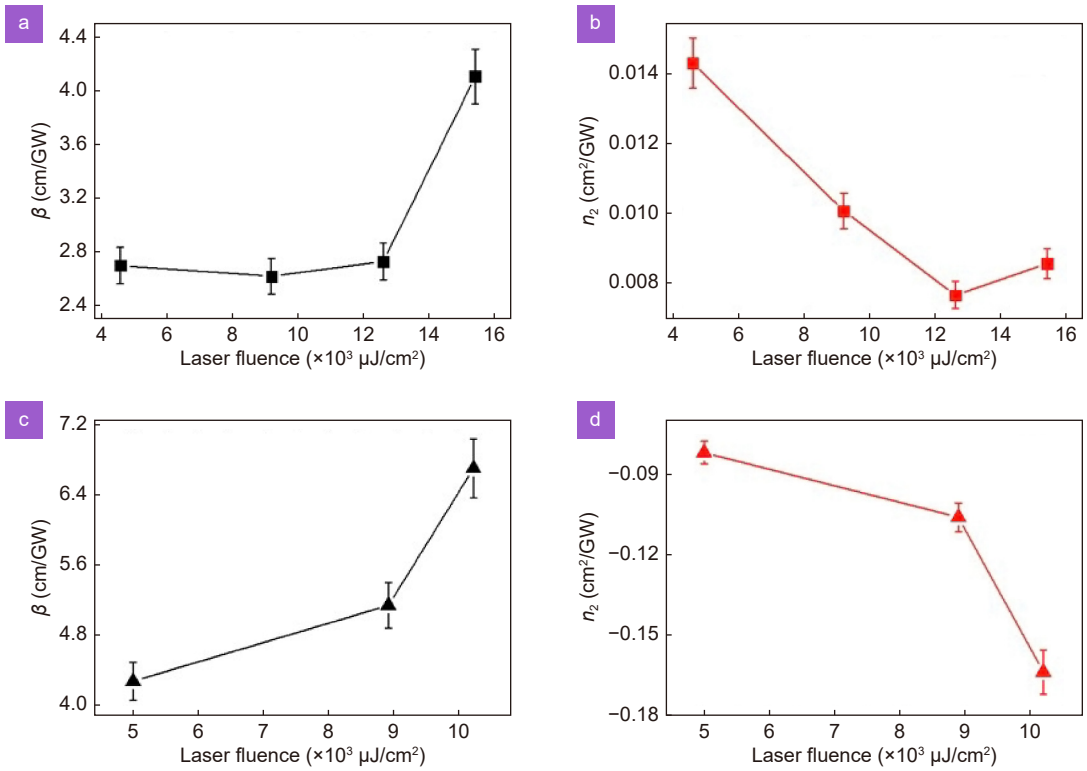

Fig. 5 | (**a**) The measured nonlinear absorption coefficient β and (**b**) nonlinear refractive index n_2 of the pristine h-BN film. (**c**) The measured nonlinear absorption coefficient β and (**d**) nonlinear refractive index n_2 of the laser oxidized h-BN film.

$$n_{2\mathrm{exc}} = -\frac{e^2\lambda^2}{8\pi^2c^2\varepsilon_0 n_0}\left(\frac{1}{m_{ce}^*}+\frac{1}{m_{ch}^*}\right)\frac{\Delta N}{I_0}, \tag{7}$$

where ε_0 is the vacuum permittivity, ΔN is the carrier density, I_0 is the peak intensity, m_{ce}^* and m_{ch}^* are the effective masses of the electron and hole respectively[49].

It is worth mentioning that the thickness of the film only decreases slightly from 3 μm to 2.7 μm after the laser oxidation (around 10%). Therefore, the overall device design can be maintained. The calculated results of β and n_2 together with the third-order susceptibility $\chi^{(3)}$ are presented in Table 1, where the absolute value of the third-order nonlinear optical susceptibility was calculated as:

$$\left|\chi^{(3)}\right| = \left[\left(\mathrm{Re}(\chi^{(3)})\right)^2+\left(\mathrm{Im}(\chi^{(3)})\right)^2\right]^{\frac{1}{2}}. \tag{8}$$

The real and imaginary parts of $\chi^{(3)}$ in the international system (SI) units are the following equations:

$$\mathrm{Re}\left|\chi^{(3)}\right| = \left(\frac{4}{3}\right)n_0^2\varepsilon_0 c n_2, \tag{9}$$

$$\mathrm{Im}\left|\chi^{(3)}\right| = (n_0^2\varepsilon_0 c\lambda/3\pi)\beta, \tag{10}$$

where n_0, ε_0, c and λ stand for the linear refraction index of the material, the electric permittivity of free space, the speed of light in vacuum and the light wavelength.

The h-BN film shows strong third-order nonlinear refraction with a largest n_2~0.0143 cm²/GW, as summarized in Table 1 below, which is ten orders of magnitude higher than the h-BN material made by liquid exfoliation (n_2~1.2×10⁻¹³ cm²/GW), and 60 times smaller than that of CVD made h-BN but at the benefit of transfer free. The ultrahigh nonlinearity provides a promising thin-film platform for practical nonlinear applications.

After laser irradiation (Fig. 5(c) and 5(d)), β is found to increase slightly than that of the pristine state.

Table 1 | The compared results of different kinds of h-BN with their nonlinear absorption coefficient β, nonlinear refractive index n_2, the imaginary part Im$\chi^{(3)}$ and the real part Re$\chi^{(3)}$ and the effective third-order susceptibility $|\chi^{(3)}|$ of complex third-order susceptibility $\chi^{(3)}$.

Material	β (cm/GW)	n_2 (cm²/GW)	Im($\chi^{(3)}$) (×10⁻¹² esu)	Re($\chi^{(3)}$) (×10⁻⁹ esu)	$\lvert\chi^{(3)}\rvert$ (×10⁻⁹ esu)	FoM	Reference
Liquid exfoliated h-BN nanosheets	74.84	1.2×10⁻¹³	NA	NA	NA	NA	ref.[23]
Monolayer CVD h-BN	10⁴	10	NA	NA	NA	NA	ref.[24]
Chemical-weathering h-BN	0.079	NA	NA	NA	NA	NA	ref.[50]
Free-standing h-BN (pristine)	4.11	0.0086	4.11	16.38	16.38	26.15	Our work
Free-standing h-BN (laser oxidized)	6.71	0.1638	4.85	11.84	11.84	305.14	Our work

However, n_2 not only flips the sign from positive to negative but also exhibits significantly enhanced values compared to those of the pristine film. It is worth mentioning that after laser irradiation, n_2 is as large as 0.1638 cm^2/GW, and the third-order nonlinear susceptibility of the oxidized h-BN film has been found to be 11.84×10^{-9} esu, which is 20 times larger than the value obtained for a pristine film[23]. Given the fact of the almost unchanged nonlinear absorption, the nonlinear figure of merit (FoM) is enhanced by 17 times. More interestingly, due to the comparatively low nonlinear absorption (3 orders of magnitude lower than the CVD h-BN film) and high nonlinear refraction, the derived nonlinear FoM for the free-standing h-BN film is one order of magnitude higher than the CVD h-BN, making it more attractive for all optical communication applications.

To exploit the third order nonlinearity, we developed the FWM-based wavelength conversion system to measure the frequency conversion efficiency of h-BN film[51]. Two incident pump laser beams with frequency ω_1 and ω_2 were focused onto the h-BN film by a microscopic objective (100×, 0.85 NA). The powers for the two incident lasers were both at 40 mW. They were mixed together to generate a third beam at frequency $\omega_e=2\omega_1-\omega_2$.[51] When being pumped by wavelengths λ_1=865 nm (ω_1, generated by a Ti: Sapphire pump laser, 80 MHz repetition rate), and λ_2=1200 nm (ω_2, generated by an optical parametric oscillator by the same pump laser) at the same time, a clear resonant spike in emission at $\lambda_e\approx$676 nm was observed, corresponding to the frequency ω_e, as shown in Fig. 6 (red line). Compared with a well-characterized, quasi-2D material of gold thin film, whose effective nonlinear susceptibility $\chi^{(3)}$ is about 4×10^{-9} esu[52], the amplitude of the emission peak of h-BN is seven times higher than that of the gold film under the same experimental conditions (shown in Fig. 6 black line). We can retrieve the effective nonlinear susceptibility to be approximately $|\chi^{(3)}|\approx2.15\times10^{-8}$ esu, showing the exceptionally high third-order nonlinear response in our all solid-state h-BN film and match very well with the Z-scan measurement. More importantly, compared with other well-studied 2D materials and semiconductor materials, such as graphene, $MoSe_2$, MoS_2, WSe_2, WS_2, GaAs, Si, SnS_2, h-BN free-standing film shows its obvious advantage in optical nonlinear and integrated photonics[53].

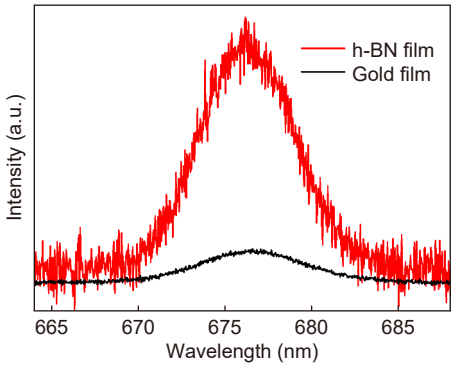

Fig. 6 | FWM spectra of the h-BN film excited with pump wavelengths (865 nm, 1200 nm), compared to that of a standard gold film.

Conclusions

In summary, free-standing h-BN film is an important and versatile optical material platform for micro- and nano- nonlinear photonics. The measured susceptibility is as high as ~10^{-8} esu, which has been both characterized by FWM and Z-scan methods. We demonstrate a technique to continuously control the third-order nonlinearity of the free-standing h-BN film by localized laser oxidation, which yields an unprecedented enhancement (more than 20 times) in the third-order nonlinearity, especially for n_2. Meanwhile, the oxidation mechanism has been revealed by FTIR spectra and Raman spectra. These results indicate *via* localized laser beam can swiftly improve the versatility of free-standing h-BN film. The laser micropatterning capability and the giant and modified nonlinearity render the free-standing h-BN film a promising platform material towards state-of-the-art nonlinear functional devices for telecommunication, such as optical switchers, wavelength converters and signal regenerators, also pave the way for simple modification towards the all solid-state applications.

References

1. Novoselov KS, Geim AK, Morozov SV, Jiang D, Zhang Y et al. Electric field effect in atomically thin carbon films. *Science* **306**, 666–669 (2004).
2. Zheng XR, Xu B, Li S, Lin H, Qiu L et al. Free-standing graphene oxide mid-infrared polarizers. *Nanoscale* **12**, 11480–11488 (2020).
3. Zheng XR, Jia BH, Lin H, Qiu L, Li D et al. Highly efficient and ultra-broadband graphene oxide ultrathin lenses with three-dimensional subwavelength focusing. *Nat Commun* **6**, 8433 (2015).
4. Lin H, Lin KT, Yang TS, Jia BH. Graphene multilayer photonic metamaterials: fundamentals and applications. *Adv Mater Technol* **6**, 2000963 (2021).
5. Lin KT, Lin H, Yang TS, Jia BH. Structured graphene metamaterial selective absorbers for high efficiency and omnidirectional solar thermal energy conversion. *Nat Commun* **11**, 1389 (2020).

6. Lin H, Sturmberg BCP, Lin KT, Yang YY, Zheng XR et al. A 90-nm-thick graphene metamaterial for strong and extremely broadband absorption of unpolarized light. *Nat Photonics* **13**, 270–276 (2019).
7. Wei SB, Cao GY, Lin H, Yuan XC, Somekh M et al. A varifocal graphene metalens for broadband zoom imaging covering the entire visible region. *ACS Nano* **15**, 4769–4776 (2021).
8. Wei SB, Cao GY, Lin H, Mu HR, Liu WB et al. High tolerance detour-phase graphene-oxide flat lens. *Photonics Res* **9**, 2454–2463 (2021).
9. Lin H, Xu ZQ, Cao GY, Zhang YP, Zhou JD et al. Diffraction-limited imaging with monolayer 2D material-based ultrathin flat lenses. *Light:Sci Appl* **9**, 137 (2020).
10. Li XY, Wei SB, Cao GY, Lin H, Zhao YJ et al. Graphene metalens for particle nanotracking. *Photonics Res* **8**, 1316–1322 (2020).
11. Zhou CH, Cao GY, Gan ZX, Ou QD, Chen WJ et al. Spatially modulating the fluorescence color of mixed-halide perovskite nanoplatelets through direct femtosecond laser writing. *ACS Appl Mater Interfaces* **11**, 26017–26023 (2019).
12. Cao GY, Lin H, Fraser S, Zheng XR, Del Rosal B et al. Resilient graphene ultrathin flat lens in aerospace, chemical, and biological harsh environments. *ACS Appl Mater Interfaces* **11**, 20298–20303 (2019).
13. Cao GY, Gan XS, Lin H, Jia BH. An accurate design of graphene oxide ultrathin flat lens based on Rayleigh-Sommerfeld theory. *Opto-Electron Adv* **1**, 180012 (2018).
14. Hu QM, Lin KT, Lin H, Zhang YY, Jia BH. Graphene metapixels for dynamically switchable structural color. *ACS Nano* **15**, 8930–8939 (2021).
15. Wang ZY, Yang TS, Zhang YP, Ou QD, Lin H et al. Flat lenses based on 2D perovskite nanosheets. *Adv Mater* **32**, 2001388 (2020).
16. Kubota Y, Watanabe K, Tsuda O, Taniguchi T. Deep ultraviolet light-emitting hexagonal boron nitride synthesized at atmospheric pressure. *Science* **317**, 932–934 (2007).
17. Watanabe K, Taniguchi T, Kanda H. Direct-bandgap properties and evidence for ultraviolet lasing of hexagonal boron nitride single crystal. *Nat Mater* **3**, 404–409 (2004).
18. Nebel CE. Light sources: tackling the deep ultraviolet. *Nat Photonics* **3**, 564–566 (2009).
19. Kim S, Fröch JE, Christian J, Straw M, Bishop J et al. Photonic crystal cavities from hexagonal boron nitride. *Nat Commun* **9**, 2623 (2018).
20. Caldwell JD, Aharonovich I, Cassabois G, Edgar JH, Gil B et al. Photonics with hexagonal boron nitride. *Nat Rev Mater* **4**, 552–567 (2019).
21. Ismach A, Chou H, Ferrer DA, Wu YP, McDonnell S et al. Toward the controlled synthesis of hexagonal boron nitride films. *ACS Nano* **6**, 6378–6385 (2012).
22. Li YL, Rao Y, Mak KF, You Y, Wang SY et al. Probing symmetry properties of few-layer MoS_2 and h-BN by optical second-harmonic generation. *Nano Lett* **13**, 3329–3333 (2013).
23. Kim S, Fröch JE, Gardner A, Li C, Aharonovich I et al. Second-harmonic generation in multilayer hexagonal boron nitride flakes. *Opt Lett* **44**, 5792–5795 (2019).
24. Popkova AA, Popkova IM, Fröch JE, Kim S, Kim I et al. Optical third-harmonic generation in hexagonal boron nitride thin films. *ACS Photonics* **8**, 824–831 (2021).
25. Lei WW, Mochalin VN, Liu D, Qin S, Gogotsi Y et al. Boron nitride colloidal solutions, ultralight aerogels and freestanding membranes through one-step exfoliation and functionalization. *Nat Commun* **6**, 8849 (2015).
26. Zhang SL, Liu LW, Ren S, Li ZL, Zhao YH et al. Recent advances in nonlinear optics for bio-imaging applications. *Opto-Electron Adv* **3**, 200003 (2020).
27. Rahmani M, Leo G, Brener I, Zayats AV, Maier SA et al. Nonlinear frequency conversion in optical nanoantennas and metasurfaces: materials evolution and fabrication. *Opto-Electron Adv* **1**, 180021 (2018).
28. Yang TS, Lin H, Jia BH. Ultrafast direct laser writing of 2D materials for multifunctional photonics devices. *Chin Opt Lett* **18**, 023601 (2020).
29. Wang HT, Hao CL, Lin H, Wang YT, Lan T et al. Generation of super-resolved optical needle and multifocal array using graphene oxide metalenses. *Opto-Electron Adv* **4**, 200031 (2021).
30. Zhao G, Zhang F, Wu YZ, Hao XP, Wang ZP et al. One-step exfoliation and hydroxylation of boron nitride nanosheets with enhanced optical limiting performance. *Adv Opt Mater* **4**, 141–146 (2016).
31. Li LH, Cervenka J, Watanabe K, Taniguchi T, Chen Y. Strong oxidation resistance of atomically thin boron nitride nanosheets. *ACS Nano* **8**, 1457–1462 (2014).
32. Zheng XR, Jia BH, Chen X, Gu M. In situ third-order non-linear responses during laser reduction of graphene oxide thin films towards on-chip non-linear photonic devices. *Adv Mater* **26**, 2699–2703 (2014).
33. Ren J, Zheng XR, Tian ZM, Li D, Wang P et al. Giant third-order nonlinearity from low-loss electrochemical graphene oxide film with a high power stability. *Appl Phys Lett* **109**, 221105 (2016).
34. Fraser S, Zheng XR, Qiu L, Li D, Jia BH. Enhanced optical nonlinearities of hybrid graphene oxide films functionalized with gold nanoparticles. *Appl Phys Lett* **107**, 031112 (2015).
35. Jia YC, Wang SX, Chen F. Femtosecond laser direct writing of flexibly configured waveguide geometries in optical crystals: fabrication and application. *Opto-Electron Adv* **3**, 190042 (2020).
36. Xie XZ, Zhou CX, Wei X, Hu W, Ren QL. Laser machining of transparent brittle materials: from machining strategies to applications. *Opto-Electron Adv* **2**, 180017 (2019).
37. Zheng XR, Lin H, Yang TS, Jia BH. Laser trimming of graphene oxide for functional photonic applications. *J Phys D:Appl Phys* **50**, 074003 (2017).
38. Guo L, Shao RQ, Zhang YL, Jiang HB, Li XB et al. Bandgap tailoring and synchronous microdevices patterning of graphene oxides. *J Phys Chem C* **116**, 3594–3599 (2012).
39. Nair RR, Blake P, Grigorenko AN, Novoselov KS, Booth TJ et al. Fine structure constant defines visual transparency of graphene. *Science* **320**, 1308 (2008).
40. Yang YY, Lin H, Zhang BY, Zhang YN, Zheng XR et al. Graphene-based multilayered metamaterials with phototunable architecture for on-chip photonic devices. *ACS Photonics* **6**, 1033–1040 (2019).
41. Lu JP, Wu J, Carvalho A, Ziletti A, Liu HW et al. Bandgap engineering of phosphorene by laser oxidation toward functional 2D materials. *ACS Nano* **9**, 10411–10421 (2015).
42. The properties of glass. By G. W. Morey, Pp, 561. New York; Reinhold Publishing Corp.; London: chapman & Hall, Ltd., 1938.62s. 6d. *J Soc Chem Ind* **58**, 422 (1939).

43. Li PF, Chen Y, Yang TS, Wang ZY, Lin H et al. Two-dimensional $CH_3NH_3PbI_3$ perovskite nanosheets for ultrafast pulsed fiber lasers. *ACS Appl Mater Interfaces* **9**, 12759–12765 (2017).
44. Yang TS, Abdelwahab I, Lin H, Bao Y, Tan SJR et al. Anisotropic third-order nonlinearity in pristine and lithium hydride intercalated black phosphorus. *ACS Photonics* **5**, 4969–4977 (2018).
45. Tan SJR, Abdelwahab I, Ding ZJ, Zhao XX, Yang TS et al. Chemical stabilization of 1T′ phase transition metal dichalcogenides with giant optical Kerr nonlinearity. *J Am Chem Soc* **139**, 2504–2511 (2017).
46. Kumbhakar P, Kole AK, Tiwary CS, Biswas S, Vinod S et al. Nonlinear optical properties and temperature-dependent UV–Vis absorption and photoluminescence emission in 2D hexagonal boron nitride nanosheets. *Adv Opt Mater* **3**, 828–835 (2015).
47. Sheik-Bahae M, Said AA, Van Stryland EW. High-sensitivity, single-beam n_2 measurements. *Opt Lett* **14**, 955–957 (1989).
48. Lu SB, Zhao CJ, Zou YH, Chen SQ, Chen Y et al. Third order nonlinear optical property of Bi_2Se_3. *Opt Express* **21**, 2072–2082 (2013).
49. Spano R, Daldosso N, Cazzanelli M, Ferraioli L, Tartara L et al. Bound electronic and free carrier nonlinearities in Silicon nanocrystals at 1550nm. *Opt Express* **17**, 3941–3950 (2009).
50. Termoss H, Toury B, Pavan S, Brioude A, Bernard S et al. Preparation of boron nitride-based coatings on metallic substrates via infrared irradiation of dip-coated polyborazylene. *J Mater Chem* **19**, 2671–2674 (2009).
51. Xia CQ, Zheng CX, Fuhrer MS, Palomba S. Nonlinear optical frequency mixing response of single and multilayer graphene. *Opt Lett* **41**, 1122–1125 (2016).
52. Hendry E, Hale PJ, Moger J, Savchenko AK, Mikhailov SA. Coherent nonlinear optical response of graphene. *Phys Rev Lett* **105**, 097401 (2010).
53. Autere A, Jussila H, Dai YY, Wang YD, Lipsanen H et al. Nonlinear optics with 2D layered materials. *Adv Mater* **30**, 1705963 (2018).

Acknowledgements

We are grateful for financial supports from the Australian Research Council through the Discovery Project scheme (Grant No. DP190103186 and FT210100806), and the Australian Research Council through Industrial Transformation Training Centres scheme (IC180100005).

Author contributions

J. Ren has guided the third order nonlinearity measurement and built up the Z-scan experiment; X. R. Zheng has participated in the four wave mixing experiment; H. Lin helped to revise the paper, W. W. Lei and D. Liu supplied the h-BN materials; T. L. Ren, P. Wang and B. H. Jia have guided the whole work, data analyses. All the authors have commented on the manuscript.

Competing interests

The authors declare no competing financial interests.